Dynamic Second-Skin Façade Systems: Numerical Energy Performance and Life Cycle Assessment of 3D-Printed Panels in a Norwegian Case Study

Luigi Tufano[1][*], Juudit Ottelin[2], Alessandro Nocente[3], Julia Sborz[2], Michelangelo Scorpio[1], Sergio Sibilio[1], Giovanni Ciampi[1]

[1] Department of Architecture and Industrial Design, University of Campania Luigi Vanvitelli, 81100 Caserta, Italy
[2] Industrial Ecology Programme, Department of Energy and Process Engineering, Norwegian University of Science and Technology (NTNU), 7491 Trondheim, Norway
[3] SINTEF AS, 7491 Trondheim, Norway

[*] Correspondence: Luigi Tufano (luigi.tufano@unicampania.it)

Abstract: In a global context where buildings account for approximately 30% of final energy demand and 26% of energy-related greenhouse gas emissions, improving the building envelope is a key strategy for achieving sustainability goals. This study investigates the energy, environmental and visual performance of a dynamic Second-Skin Façade (SSF) system applied as a passive retrofit solution for a typical office building located in Trondheim, Norway. The SSF integrates adaptive technologies and is composed of 3D-printed panels in Acrylonitrile Styrene Acrylate (ASA): solid panels for opaque walls and perforated panels for windows. A simulation-based methodology using TRNSYS software was implemented to compare the performance of the retrofitted building against a reference case. Additionally, a gate-to-gate Life Cycle Assessment was performed to assess the environmental impact of the 3D-printed components. Results highlight a reduction in primary energy demand by up to 25.5% and an annual decrease of approximately 1.4 tCO_{2eq}, particularly when the dynamic shading control is based on vertical solar radiation. Although the Global Warming Potential of ASA panels is higher than that of conventional materials, the local production and Norway's low-carbon electricity grid contribute to a favorable environmental profile. The findings underline the potential of 3D printing for adaptive envelope solutions.

Keywords: Building envelope; Dynamic shading; Façade retrofit; Office building; 3D print

1 Introduction

Currently, buildings are responsible for nearly 30% of global energy consumption and account for approximately 26% of worldwide carbon emissions [1]. To address this issue, the European Union has introduced long-term goals aimed at lowering greenhouse gas emissions by 2050 [2]. A substantial portion of the non-residential buildings across the EU were constructed before 1990, and approximately 55% of this stock remains unrenovated [3, 4]. In Norway, about half of the existing commercial buildings were constructed between 1981 and 2010 [5–7]. This implies that the majority of commercial structures in these regions are neither very old nor brand-new, but of medium age (often corresponding to the era of building codes from the 1980s, 90s, and 2000s). It should be noted that when considering floor area or volume, the influence of post-1980 buildings could be even greater, as newer commercial buildings (such as large shopping malls or office complexes built in the 2000s) generally have a larger floor space than early 20th-century shops or warehouses. Regionally, the breakdown by county aligns with the above: for instance, Trøndelag (Central Norway) has about 55% of its commercial buildings built 1981–2010, while Agder (Southern Norway) is around 50% [5–7]. In Northern Norway, which comprises the counties of Nordland, Troms, and Finnmark, approximately 45% to 50% of the current commercial building stock was constructed between 1981 and 2010. Since major cities in these regions followed suit and saw extensive development in the late 20th century, a large proportion of their commercial building stock dating from the same period. Overall, official statistics confirm

that the commercial building stocks in central and southern Norway are dominated by structures built between 1981 and 2010, accounting for roughly half to a little over half of all commercial buildings in each region [5–7]. Consequently, there is growing government support for retrofit strategies aimed at enhancing building energy efficiency. These retrofit interventions can be categorized into two broad categories: active and passive [8, 9]. Active strategies incorporate technologies that enhance energy efficiency, whereas passive strategies aim to reduce energy consumption by regulating thermal exchanges and maximizing the benefits of natural lighting, heating, or cooling. Among passive methods, the building envelope is a crucial component [8, 9]. However, retrofitting the envelope by replacing glazing or improving insulation is not always feasible due to heritage constraints or cost limitations [10]. In such cases, the application of a non-invasive, lightweight, and low-maintenance external Second-Skin Façade (SSF) system can serve as a viable alternative to improve thermal performance. SSF systems offer an efficient balance between cost, performance, and installation simplicity [10]. These systems typically consist of a secondary external layer separated from the main façade by an air gap. Due to their structural simplicity, SSF system can easily incorporate various materials, including innovative light-weight components [8–15]. Nonetheless, research into SSF systems in cold climates remains limited, particularly regarding the use of 3D-printed materials in such regions. Despite this, these innovative materials are becoming increasingly popular in modern architectural applications thanks to their lightweight, adaptability, and aesthetic flexibility in both new construction and renovations, offering thermal benefits that support passive heating and cooling, which in turn helps to reduce energy usage and carbon emissions [9, 10, 16].

This paper aims to evaluate the impact of passive retrofit actions on a typical office building in terms of energy, environmental, and visual comfort from a Nordic climate perspective, aiming to address the gaps in this region. The analysis was carried out using the dynamic simulation software TRNSYS 18 [17] comparing the results of a reference office building with those achievable by adopting a passive retrofit action on the building envelope across a whole year. In particular, the refurbishment consists of installing a dynamic Second-Skin Façade system realized with two types of 3D-printed panels: (i) opaque solid panels on wall surfaces and (ii) perforated ones on openings, both realized in Acrylonitrile Styrene Acrylate (ASA) [18].

2 Material and Methods

This section outlines the methodological framework used to evaluate the integration of the SSF system into the selected building model, including its energy and environmental impacts. The approach is structured into three main phases. First, a representative building model is defined and characterized (Section 2.1), serving as the baseline for simulation and comparative analysis. Second, the SSF system, its design, configuration, and operational principles, is described in detail (Section 2.2). Lastly, energy, environmental and visual comfort analyses are described in detail (Section 2.3).
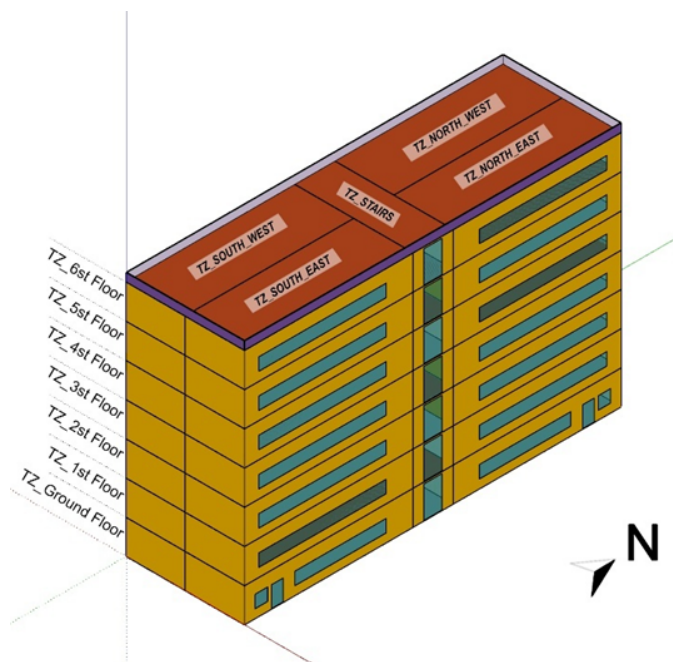
2.1 Building Model

Figure 1. Axonometric view of the building model in orientations east-west

The study focuses on an office building. It aims to propose a general operational methodology and highlight a best practice for retrofit actions in the Norwegian context. The software TRNSYS 18 has been used to evaluate the potential benefit achievable in an office building refurbishment using a 3D-print material (ASA) as the outer layer in an SSF system in terms of primary energy saving and reduction of carbon dioxide equivalent emissions. The reference building investigated in this research has been modeled in SketchUp 3D-modeling software based on a "typical" office building from the IEA Annex 27 activity [19]. It is a seven-story building 45.9 m wide, 14.4 m deep, and 28.9 m tall. Figure 1 reports the simulated building, highlighting the Thermal Zones (TZs) per floor. In particular, the geometrical model was realized using SketchUp 3D-modeling software, dividing each floor into five TZs upon varying the space typology, office or stairs, and the orientation, east or west.

The windows were implemented only on the two main façades, considering the optimal Windows-to-Wall Ratio (WWR) as suggested by [20] and equal to 33% and 34% for the East façade and the West façade, respectively.

The geometrical model was then imported into TRNSYS to characterize the envelope (all surfaces are modeled as massless), the internal gains, and the setpoints for the cooling and heating systems. The study was carried out considered the building located in Trondheim (63°26'24"N, 10°24'0"E), central Norway.

The most common building typology of the Norwegian building stock has been modeled as a reference building [21], classified as a medium-aged building (built between 1981 and 2010). The envelope of this building typology has been characterized differently in terms of thermal transmittance (U-value), according to its age and contemporary building regulations [21]. Table 1 summarizes the implemented U-values. In TRNSYS, the reference building has been simulated through Type 56.

Table 1. U-values considered for the reference building

Construction	U-values (W/m^{2}K)
Wall	0.30
Roof	0.20
Floor	0.30
Windows	2.40

Table 2 lists the common simulation parameters [20, 22–25]. In addition, experimental data acquired from June 1st (2021) to May 31st (2022) were used to take into account the real weather conditions. Data were acquired by the weather station integrated into the ZEB Test Cell experimental facility in Trondheim.

The experimental weather conditions were acquired with one-minute temporal resolution and averaged over 15 minutes.
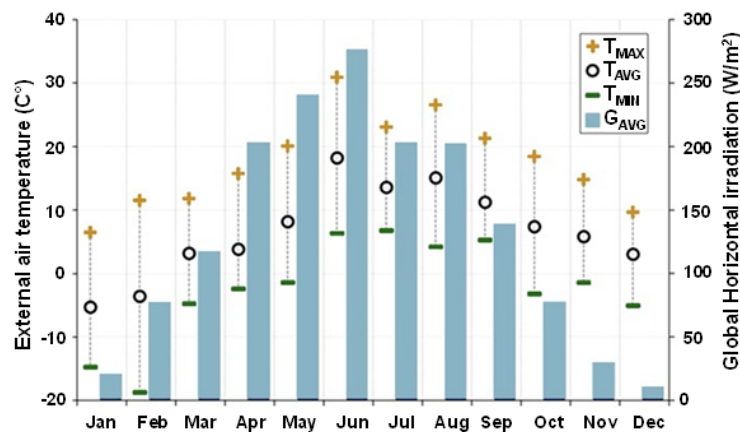

Figure 2. Values of TMAX, TMIN, TAVG, and GAVG for each simulation month

Figure 2 presents the maximum (TMAX), minimum (TMIN), and average (TAVG) values of the outdoor air temperature, as well as the average global horizontal irradiation (GAVG), for varying months. This figure highlights that: (i) the outdoor air temperature ranges between a minimum of -18.75°C in February and a maximum of 30.94°C in June, (ii) the average global horizontal irradiation is minimum in December (9.72 W/m^2), while the value of GAVG is maximum in June (275.31 W/m^2). In addition, the experimental weather data shows that July 2021 was particularly cloudy.

A preliminary simulation set was run in order to assess the thermal and cooling loads across the whole year for both buildings' typologies and orientations to choose a proper size for the heating and cooling systems. Thus,

commercial electric heat pump [24, 25] devices (see Table 2), coupled with a multi-split air conditioning system, were implemented for each TZ to supply the required heating and cooling energy.

Table 2. Summary of the simulations' parameters

Parameter	Detail	Value
Occupancy	Workhours	8:00–11:30
		12:30–16:00
Office heating system	Temperature setpoint	20℃
	Lunchbreak/Nightime/weekend	15℃
	COP (mod. Clint CHA/F/ML/WP 62)	2.71
Office cooling system	Temperature setpoint	26℃
	Lunchbreak/Nightime/weekend	30℃
	EER (mod. Clint CHA/F/ML/WP 62)	3.10
Stair heating system	Temperature setpoint	20℃
	Lunchbreak/Nightime/weekend	15℃
	COP (mod. Clint CHA/IG/A/WP 61)	3.29
Stair cooling system	Temperature setpoint	26℃
	Lunchbreak/Nightime/weekend	30℃
	EER (mod. Clint CHA/IG/A/WP 61)	2.75
Lighting system	Workhours	8.0 W/m^2
	Lunchbreak	2.4 W/m^2
	Nightime/weekend	0.0 W/m^2
Equipment	Workhours	11.0 W/m^2
	Lunchbreak	6.6 W/m^2
	Nightime/weekend	1.1 W/m^2
People	Workhours	7.0 W/m^2
	Lunchbreak	2.1 W/m^2
	Nightime/weekend	0.0 W/m^2

2.2 Dynamic SSF System

In the refurbishment cases, a dynamic SSF system (consisting of the SSF external layer, a 10 cm wide air cavity, and an insulation layer on the outer surface of the existing exterior wall) integrating the 3D-print material as the external layer has been implemented on the whole reference building's walls (Figure 3). Two types of ASA 3D-printed panels (the size of each panel is 60 cm × 60 cm × 1.5 cm) were considered for installation on the opaque and transparent building envelope: a solid panel (Figure 4, red marker) and a perforated panel with 28% porosity (Figure 4, blue marker) [9, 10].

The SSF system was implemented in TRNSYS through Type 1230. This TRNSYS Type, coupled with Type 56 reproduces the behavior of the external second-skin layer with the 10 cm wide air cavity. In particular, the external layer of the building wall (modeled with Type 56), usually an insulation layer, acts as an interface layer between the two Types by coupling its temperature and thermal resistance to model the wall heat transfer. Type 1230 takes into account the following factors: (i) solar radiation, long-wave radiation, and air convection on the external surface of the outer layer; (ii) energy storage and conduction within the outer layer; (iii) radiation exchange between the outer layer and the air cavity; (iv) convective exchanges from all surfaces that face the air cavity; and (v) conduction through the interface layer. More details about Type 1230 can be found in reference [10]. In particular, in reference [10] the authors calibrated and validated the numerical model of the SSF system used in this research based on experimental data collected in the southern Italian climate. The comparison between the experimental and the numerical data demonstrated good reliability of this numerical model, with an RMSE of 0.4℃ and 0.2℃ for the indoor air temperature and the temperature of the air cavity, respectively [10]. In this paper, the insulation layer (Expanded PolyStyrene—EPS, l = 0.041 W/mK) was set equal to 0.051 m in order to meet the U-value threshold of 0.22 W/m^{2}K specified by current legislation on the performance of the building envelope [26].

The 3D printed panels were realized by using the Stratasys F900 3D printer [27] with the Fused Deposition Modeling (FDM) technology, considering a 20% Gyroid filling. The thermal properties of the solid panel were experimentally derived by using the Hot Disk Thermal Constants Analyser (TPS 1000) as described in reference [28]. In particular, the experimental results showed a thermal conductivity equal to 0.0249 W/mK [28].

Figure 3. Comparison between the reference (RC) and the refurbished (SSF) office building
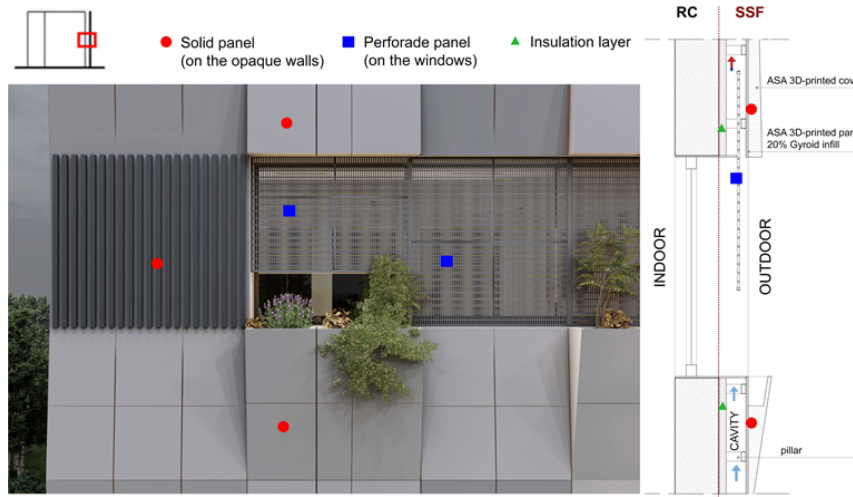

Figure 4. ASA 3D-printed panels used for the dynamic SSF system in the retrofit and section of SSF system layout

The perforated panels can be moved to cover or uncover the windows, allowing for independent control of each TZ. Two different retrofit cases with two control strategies were simulated:

• Case RG50. when the control is based on the vertical solar irradiation (VG) threshold on the façades;

• Case RILL, when the control is based on the indoor horizontal illuminance values (HILL) at 0.80 m from the floor.

Figure 5 shows the layout of 34 horizontal illuminance (HILL) measurement points located at a height of 0.80 m from the floor to evaluate visual comfort across the different TZs on the 3rd floor. The other floors maintain a similar configuration.
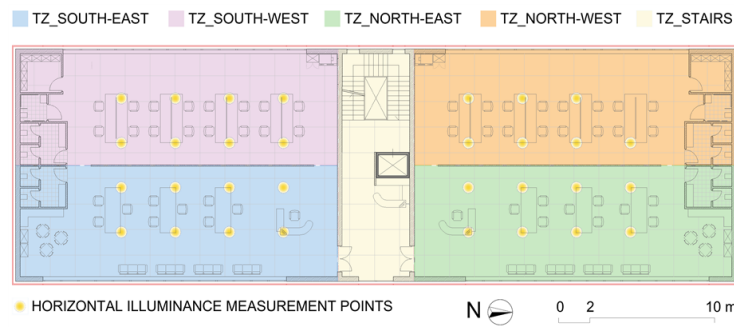

Figure 5. Layout of the HILL points for each floor

In this study, the changes in infiltration rates were assumed based on literature references [29–31]: (i) both the SSF sections in front of the windows and the shutters are open, so the air infiltration rate is equal to 1.5 m³/h; (ii) both are closed, so the air infiltration rate is 0.6 m³/h; (iii) in case one is open the air infiltration rate is equal to 1.5 m³/h. These assumptions could be the main limitation of this work. According to reference [32], air infiltration through the building envelope, driven by pressure differences between the interior and the façade, can be significantly affected

by changes in the envelope's geometry and material composition. In this context, the study presented here represents an initial step toward a broader experimental investigation. Currently, only experimental weather data for a northern location was available, whereas the numerical model of the SSF system incorporating 3D-printed materials was developed and validated in Southern Europe [10]. Further experimental analysis is required in the Nordic Region to assess the influence of different boundary conditions and the effects on the overall balance from a fluid-dynamic perspective.

Table 3 presents the operative states in the two different control strategies adopted for opening/closing the dynamic shading system of the SSF (first letter of the state, O = open and C = closed) and the shutters of the air cavity (second letter of the state, O = open and C = closed).

Table 3. Summary of operative states for the adopted control strategies

Sate	Control Logic 1 for SSF (V_G)	Control Logic 2 for SSF (H_{ILL})	Air Cavity Shutters	Infiltration Rate (m^3/h)
OO	$V_G < 50$ W/m2	$H_{ILL} < 2000$ lux	$T_{air} > 20°C$	1.5
CC	$V_G \geq 50$ W/m2	$H_{ILL} \geq 2000$ lux	$T_{air} \leq 20°C$	0.6
OC	$V_G < 50$ W/m2	$H_{ILL} < 2000$ lux	$T_{air} \leq 20°C$	1.5
CO	$V_G \geq 50$ W/m2	$H_{ILL} \geq 2000$ lux	$T_{air} > 20°C$	1.5

2.3 Energy, Environmental and Visual Analyses

The energy comparison between the proposed cases (PC) and the reference case (RC) has been performed considering the primary energy consumption through the index PES (Primary Energy Saving) [10, 33]:

$$PES = \left[\left(E_p^{RC} - E_p^{PC} \right) / E_p^{RC} \right] \tag{1}$$

where, E_p^{RC} is the primary energy associated with the RC , while E_p^{PC} is the primary energy associated with each PC and η_{PP} (the power plants' average efficiency, including the transmission losses) is assumed equal to 0.78 according to reference [34], while the values of COP and EER are reported in Table 2. When this index is positive, it indicates that the proposed refurbishment actions result in reduced primary energy consumption compared to the reference case.

The environmental comparison is conducted by assessing the reduction of carbon dioxide equivalent emissions (ΔCO_2), defined according to [13] and reported below:

$$\Delta CO_2 = m_{CO_2,eq}^{RC} - m_{CO_2,eq}^{PC} = \alpha \cdot \left(E_{el}^{RC} - E_{el}^{PC} \right) \tag{2}$$

where, where $m_{CO2,eq}^{RC}$ represents the mass of carbon dioxide equivalent emissions for the reference cases and $m_{CO2,eq}^{PC}$ represents the mass of carbon dioxide equivalent emissions for each of the four proposed cases,, and α is the CO_2 equivalent emission factor linked to electricity production in Norway and assumed equal to 0.015 $kgCO_{2,eq}$/kWhel [35]. When this index is positive, refurbishment actions allow for a reduction in CO2 equivalent emissions compared to the reference case.

In addition, in this study, a gate-to-gate Life Cycle Assessment (LCA) [36] was performed to evaluate the environmental impacts associated with the manufacturing and assembly phase of a façade cladding panel produced using FDM with ASA polymer. The analysis includes the preparation time, printing time, energy consumption, and material usage (ASA and SR-30 support), as realized on a Stratasys F900 3D printer [27]. The assessment follows the ISO 14040 [37] standards and is limited to the product stage modules A2–A3, in line with EN 15804. Upstream raw material production (A1) and downstream stages such as transport, installation, use, and end-of-life (A4–C4) are excluded from the system boundary. The Global Warming Potential for a single 3D-printed panel (GWPpanel) is calculated using the following equation:

$$\begin{aligned} GWP_{\text{panel}} &= \left(m_{CO_2,eq}^{ASA} + m_{CO_2,eq}^{SR-30} + m_{CO_2,eq}^{\text{Eel}} \right) / A_{\text{panel}} \\ &= \left(\beta \cdot V_{ASA} \cdot \rho_{ASA} + \chi \cdot V_{SR-30} \cdot \rho_{SR-30} + \alpha \cdot E_{\text{el,3D-printer}} \right) / A_{\text{panel}} \end{aligned} \tag{3}$$

where, $m_{CO2,eq}^{ASA}$ represents the mass of carbon dioxide equivalent emissions associated to the mass of ASA, $m_{CO2,eq}^{SR-30}$ represents the mass of carbon dioxide equivalent emissions for support material SR-30 and $m_{CO2,eq}^{Ee}$ represents the

mass of carbon dioxide equivalent emissions associated with the electric energy consumed by the Stratasys F900 3D printer. The Apanel is the area in m^2 of the 3D-printed panel (equal to 0.36 m^2 for the panel used in this work). The coefficients β and χ are the equivalent emissions factors for ASA and support material SR-30, based on secondary data from literature and industry databases and equal to 3.4 kgCO$_{2,eq}$/kg and 5.5 kgCO$_{2,eq}$/kg, respectively [38, 39], V and ρ are the volume in m^3 and the density of the material in kg/m^3 of the used materials. Therefore, results are expressed per functional unit of 1 m^2 of façade panel.

Finally, visual comfort has been evaluated considering the Continuous Daylight Autonomy (CDA) and the Useful Daylight Illuminance (UDI) [40].

The CDA represents the amount of natural light available at a given point in the space during occupied hours with an illuminance value equal to 300 lux:

$$\text{with } \text{wf}_i = \left\{ \begin{array}{ll} 1 & \text{if } \text{E}_{\text{daylight}} \geq \text{E}_{\text{limit}} \\ \frac{\text{E}_{\text{daylight}}}{\text{E}_{\text{limit}}} & \text{if } \text{E}_{\text{daylight}} < \text{E}_{\text{limit}} \end{array} \right. \tag{4}$$

where, $\text{E}_{daylight}$ is the daylight illuminance calculated at each simulation timestep i, and E_{limit} is the illuminance limit equal to 300 lux.

The UDI consists of these three different fractions (Eq. (5)):

$$\text{UDI} = \frac{\sum_i (\text{wf}_i \cdot t_i)}{\sum_i t_i} \epsilon [0,1] \left\{ \begin{array}{l} \text{UDI}_{\text{overlit}} \\ \text{with } \text{wf}_i = \left\{ \begin{array}{l} 1 \text{ if } \text{E}_{\text{daylight}} > \text{E}_{\text{upper limit}} \\ 0 \text{ if } \text{E}_{\text{daylight}} \leq \text{E}_{\text{upper limit}} \end{array} \right. \\ \text{UDI UI}_{\text{useful}} \\ \text{with } \text{wf}_i = \left\{ \begin{array}{l} 1 \text{ if } \text{E}_{\text{lower limit}} \leq \text{E}_{\text{daylight}} \leq \text{E}_{\text{upper limit}} \\ 0 \text{ if } \text{E}_{\text{daylight}} < \text{E}_{\text{lower limit}} \text{ V} \text{E}_{\text{daylight}} > \text{E}_{\text{upper limit}} \end{array} \right. \\ \text{UDI U}_{\text{underlit}} \\ \text{with } \text{w}_i = \left\{ \begin{array}{l} 1 \text{ if } \text{E}_{\text{daylight}} < \text{E}_{\text{lower limit}} \\ 0 \text{ if } \text{E}_{\text{daylight}} \geq \text{E}_{\text{lower limit}} \end{array} \right. \end{array} \right. \tag{5}$$

where, t_i is each occupied hour in a year; w_{fi} is a weighting factor depending on values of $\text{E}_{daylight}$ and the illuminance limit value (upper or lower), UDI$_{overlit}$ is the percentage of time of discomfort due to daylight supply, calculated at each simulation timestep i, above the limit (2000 lux), UDI$_{underlit}$ is the percentage of time of discomfort due to daylight supply, calculated at each simulation timestep i, under the limit (100 lux), and UDI$_{useful}$ is the percentage of time with appropriate illuminance levels.
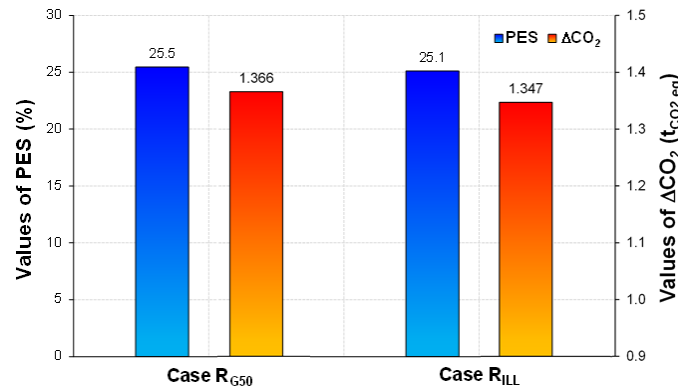
3 Results and Discussions

Figure 6. Values of PES and ΔCO$_2$

	Cooling energy for space cooling demand associated to the whole office building (kWh/m^2/year)	Thermal energy for space thermal demand associated to the whole office building (kWh/m^2/year)
Case RC	8.8	141.9
Case R$_{G50}$	5.0	79.3
Case R$_{ILL}$	7.4	77.9

Figure 7. Thermal and cooling energy demands associated with the whole office building

This section reports and discusses in detail the results of the comparison between the reference case (Case RC) and the proposed retrofit cases (Cases R_{G50} and R_{ILL}) from the perspectives of energy, environmental considerations, and indoor visual comfort. Figure 6 shows the values of PES (blue columns) and ΔCO_2 (red columns), while Figure 7 reports the thermal and cooling energy demands associated with the entire office building as the simulation case studies are varied.

Figure 6 and Figure 7 show that:

• Both the retrofit cases (Case R_{G50} and Case R_{ILL}) return positive values of PES and ΔCO_2 when compared to Case RC;

• The best results are achieved by Case R_{G50}, with a PES equal to 25.5% and about 1.4 $t_{CO2,eq}$ avoided per year; this is due to a reduction of space cooling (-43.4%) and heating (-44.1%) energy demands associated to the whole office building in comparison to Case RC;

• Although the Case R_{ILL} showed the greatest savings in terms of heating energy demand (-45.1%), this did not allow for the highest overall primary energy savings, as the reduction in cooling energy demand is about -16.0%.

The gate-to-gate LCA of the 3D-printed façade ASA panel produced locally in Norway indicates a total GWP of about 39.4 $kgCO_{2,eq}/m^2$ for the solid 3D-printed panel and about 28.3 $kgCO_{2,eq}/m^2$ for the perforated 3D-printed panel. While this value is higher than those associated with conventional cladding materials [41], such as ceramic tiles (25–30 $kgCO_{2,eq}/m^2$), aluminum composite panels (20–25 $kgCO_{2,eq}/m^2$), and high-pressure laminates (5–10 $kgCO_{2,eq}/m^2$), the localized and low-carbon production context significantly improves its environmental performance. In addition, a major advantage of the 3D-printed solution lies in its elimination of transport emissions, which can represent up to 15% of the total GWP for heavy or imported materials. Moreover, the use of Norway's largely renewable energy grid (with an electricity emission factor of 0.015 $kgCO_{2,eq}/kWh_{el}$) substantially reduces the impact of the high energy demand associated with the 43-hour printing process. Beyond carbon metrics, 3D printing offers considerable functional benefits: the ability to produce customized geometries, embed passive climate-responsive features, and integrate multiple roles (e.g., structural, aesthetic, and environmental) within a single component. It also supports modularity, on-demand production, and design for disassembly, aligning with the circular economy principles.

Table 4 lists the minimum and maximum CDA and UDI values associated with all the TZs on the third floor of the office building for all simulation cases.

Table 4. Maximum and minimum values of the visual comfort indices associated with the 3rd floor

TZ	Case	Values	CDA (%)	UDI_{useful} (%)	$UDI_{underlit}$ (%)	$UDI_{overlit}$ (%)
South_east	Case RC	Min	74.3	48.3	19.0	13.9
		Max	79.2	63.1	23.2	32.7
	Case R_{G50}	Min	27.7	34.2	28.1	0.0
		Max	54.0	71.9	65.9	0.0
	Case R_{ILL}	Min	41.0	56.3	22.3	0.0
		Max	66.3	77.2	43.7	0.2
South_west	Case RC	Min	74.0	45.3	19.25	13.6
		Max	78.9	64.2	23.52	35.4
	Case R_{G50}	Min	25.0	35.3	36.6	0.0
		Max	47.4	63.4	64.7	0.0
	Case R_{ILL}	Min	20.5	49.5	29.0	0.0
		Max	39.5	71.0	50.5	0.0
North_east	Case R_{ILL}	Min	73.6	48.1	19.2	8.1
		Max	79.1	70.3	23.5	32.8
	Case RC	Min	24.6	31.9	33.1	0.0
		Max	48.1	67.0	68.2	0.0
	Case R_{G50}	Min	40.9	54.9	24.9	0.0
		Max	62.2	75.0	45.1	0.1
North_west	Case R_{ILL}	Min	73.6	45.4	19.2	6.5
		Max	78.9	70.1	23.5	35.4
	Case RC	Min	20.5	21.7	36.0	0.0
		Max	48.4	64.0	78.4	0.0
	Case R_{G50}	Min	35.9	44.3	24.2	0.0
		Max	63.3	75.7	55.7	0.0

The other floors exhibited similar results regarding CDA and UDI values.

The simulation results reported in Table 4 show that:

• Case RC returns the best results in terms of CDA, ranging from 73.6% to 79.2%; however, the UDI$_{useful}$ index shows the lowest values ranging from 19.0% and 23.5% among all the considered cases; this is due to excessive HILL values over 2000 lux (UDI$_{overlit}$ ranges from 6.5% to 35.4%);

• Both the proposed control logics significantly increase the UDIuseful up to 71.9 and 77.2 Case R$_{G50}$ and Case R$_{ILL}$, respectively; in particular, Case R$_{ILL}$ achieves the best overall results in terms of UDI$_{useful}$, ranging from 44.3 % to 77.2%;

• In both proposed refurbishment cases using the dynamic SSF system, the values of UDI$_{overlit}$ were lower than 0.5%; therefore, the adoption of the SSF system analysed in this work highlights a slightly better uniformity of the illuminance value distributions on the whole floor.

4 Conclusions

This study examines the energy, environmental, and visual comfort performance of a dynamic SSF system that incorporates 3D-printed panels as a retrofit measure for a typical office building in Norway. Two different control logics were analyzed, considering the outdoor vertical solar irradiation and the indoor horizontal illuminance values on the desks. The results showed that the proposed retrofit action was able to improve the overall performance of the building in terms of daylight uniformity on the floor (up to 77.2%), PES, and ΔCO_2 (25.5% and 1.4 tCO$_{2,eq}$, respectively). Nonetheless, some limitations remain. The carbon footprint remains higher than that of standard materials, which is a significant limitation, particularly in regions with carbon-intensive electricity sources. In conclusion, while the 3D-printed ASA panel does not outperform conventional materials from a purely carbon standpoint, its value emerges in projects prioritizing customization, digital fabrication, local production, and smart envelope integration. In such cases, its broader sustainability potential may justify its adoption, especially when embedded in a low-impact, system-oriented architectural strategy.

Data Availability

Research data will be available on request.

Conflicts of Interest

The authors declare no conflicts of interest.

References

[1] European Commission, "Energy Performance of Buildings Directive." 2025. https://energy.ec.europa.eu/topics/energy-efficiency/energy-efficient-buildings/energy-performance-buildings-directive_en

[2] Directorate-General for Climate Action, "Building a climate-resilient future," 2023. https://climate.ec.europa.eu/news-your-voice/news/building-climate-resilient-future-2023-07-26_en

[3] ECOFYS Sustainable Energy for Everyone, "Renovation Tracks for Europe up to 2050," 2013. https://www.umweltbundesamt.de/sites/default/files/medien/377/dokumente/13_session_i_3_bettgenhaeuser.pdf

[4] ECOFYS Germany GMBH, "Is there a case for the EU to move beyond 20% GHG emissions reduction by 2020? Quantifying the impacts of a 30% target on energy security," Tech. Rep., 2011. https://climatestrategies.org/wp-content/uploads/2014/11/cs-energy-security-ecofys.pdf

[5] I. A. C. Avendano, K. H. Andersen, S. Erba, A. Moazami, M. Aghaei, and B. Najafi, "A novel framework for assessing the smartness and the smart readiness level in highly electrified non-residential buildings: A Norwegian case study," *Energy Build.*, vol. 314, p. 114234, 2024. https://doi.org/10.1016/J.ENBUILD.2024.114234

[6] Statistics Norway, "Building statistics." https://www.ssb.no/en/bygg-bolig-og-eiendom/bygg-og-anlegg/statistikk/byggeareal

[7] Statistics Norway, "Building stock." https://www.ssb.no/en/bygg-bolig-og-eiendom/bygg-og-anlegg/statistikk/bygningsmassen

[8] X. Chen, K. Qu, J. Calautit, A. Ekambaram, W. Lu, C. Fox, G. Gan, and S. Riffat, "Multi-criteria assessment approach for a residential building retrofit in Norway," *Energy Build.*, vol. 215, p. 109668, 2020. https://doi.org/10.1016/J.ENBUILD.2019.109668

[9] Y. Spanodimitriou, G. Ciampi, L. Tufano, and M. Scorpio, "Flexible and lightweight solutions for energy improvement in construction: A literature review," *Energies*, vol. 16, no. 18, p. 6637, 2023. https://doi.org/10.3390/en16186637

[10] G. Ciampi, Y. Spanodimitriou, M. Scorpio, A. Rosato, and S. Sibilio, "Energy performances assessment of extruded and 3D printed polymers integrated into building envelopes for a south Italian case study," *Buildings*, vol. 11, no. 4, p. 141, 2021. https://doi.org/10.3390/buildings11040141

[11] G. Ciampi, Y. Spanodimitriou, A. Nocente, M. Scorpio, and S. Sibilio, "Energy performances of tensile material in building renovation in the Nordic region," *E3S Web Conf.*, vol. 362, p. 05003, 2022. https://doi.org/10.1051/e3sconf/202236205003

[12] A. De Gracia, L. Navarro, A. Castell, and L. F. Cabeza, "Energy performance of a ventilated double skin facade with PCM under different climates," *Energy Build.*, vol. 91, pp. 37–42, 2015. https://doi.org/10.1016/J.ENBUILD.2015.01.011

[13] M. Gruner and M. Haase, "Façade-integrated ventilation systems in Nordic climate," in *Proceedings of the 33nd AIVC Conference "Optimising Ventilative Cooling and Airtightness for [Nearly] Zero-Energy Buildings, IAQ and Comfort"*, Copenhagen, Denmark, 2012, pp. 1–10.

[14] A. Gelesz, E. C. Lucchino, F. Goia, V. Serra, and A. Reith, "Characteristics that matter in a climate façade: A sensitivity analysis with building energy simulation tools," *Energy Build.*, vol. 229, p. 110467, 2020. https://doi.org/10.1016/J.ENBUILD.2020.110467

[15] S. Shahrzad and B. Umberto, "Parametric optimization of multifunctional integrated climate-responsive opaque and ventilated façades using CFD simulations," *Appl. Therm. Eng.*, vol. 204, p. 117923, 2022. https://doi.org/10.1016/J.APPLTHERMALENG.2021.117923

[16] L. Lopes, L. Penazzato, D. C. Reis, M. Almeida, D. V. Oliveira, and P. B. Lourenço, "A holistic modular solution for energy and seismic renovation of buildings based on 3D-printed thermoplastic materials," *Sustainability*, vol. 16, no. 5, p. 2166, 2024. https://doi.org/10.3390/su16052166

[17] TRNSYS, "Transient System Simulation Tool." http://www.trnsys.com

[18] Stratasys, "ASA FDM thermoplastic filament." https://support.stratasys.com/en/Materials/FDM/ASA

[19] International Energy Agency, "Performance, durability and sustainability of advanced windows and solar components for building envelopes," 2007. https://task27.iea-shc.org/Data/Sites/1/publications/task27-b1.pdf

[20] F. Goia, "Search for the optimal window-to-wall ratio in office buildings in different European climates and the implications on total energy saving potential," *Sol. Energy*, vol. 132, pp. 467–492, 2016. https://doi.org/10.1016/j.solener.2016.03.031

[21] N. Nord, Y. Ding, O. Skrautvol, and S. F. Eliassen, "Energy pathways for future Norwegian residential building areas," *Energies*, vol. 14, no. 4, p. 934, 2021. https://doi.org/10.3390/en14040934

[22] UNI, "Energy performance of buildings. Part 1: Evaluation of energy need for space heating and cooling," 2014. https://www.scribd.com/document/346636386/UNI-TS-11300-1-2014-pdf

[23] European Committee for Standardization, "Heating systems in buildings - Method for calculation of the design heat load," 2003. https://www.ter-en.com/book/103.pdf

[24] CLINT, "CHA/IG/A 51÷81." https://clint.it/en/products/air-cooled-liquid-chillers-and-heat-pumps-for-residential-light-commercial-application/air-cooled-liquid-chillers-and-heat-pumps/chaiga-5181/

[25] CLINT, "CHA/F/ML/WP 52÷92 ." https://clint.it/en/products/air-cooled-liquid-chillers-and-heat-pumps-for-residential-light-commercial-application/air-cooled-dedicated-heat-pumps/chafmlwp-5292/

[26] Direktoratet for Byggkvalitet, "Byggteknisk forskrift (TEK17) med veiledning," 2025. https://www.dibk.no/regelverk/byggteknisk-forskrift-tek17

[27] Stratasys, "Scheda tecnica," 2021. https://www.stratasys.com/it/

[28] L. Tufano, M. Scorpio, B. Andreozzi, A. Carola, M. Donisi, A. Rosato, and G. Ciampi, "Influence of Italian climatic conditions on performance of a 3D printed building second-skin façade with 20% gyroid filling: Simulation assessment," *Int. J. Des. Nat. Ecodyn.*, vol. 19, no. 5, pp. 1491–1499, 2024. https://doi.org/10.18280/ijdne.190503

[29] A. Dickson, "Modelling double-skin facades," University of Strathclyde, United Kingdom, 2004. https://www.esru.strath.ac.uk/Documents/MSc_2004/dickson.pdf

[30] G. Y. Cho, M. S. Yeo, and K. W. Kim, "Design parameters of double-skin façade for improving the performance of natural ventilation in high-rise residential buildings," *J. Asian Archit. Build. Eng.*, vol. 12, no. 1, pp. 125–132, 2013. https://doi.org/10.3130/jaabe.12.125

[31] M. Haase, I. Andresen, B. Time, and A. G. Hestnes, "Design and future of energy-efficient office buildings in Norway," in *Eleventh International IBPSA Conference*, Glasgow, Scotland, 2009, pp. 1872–1879.

[32] A. Darvish, S. R. Eghbali, G. Eghbali, and Y. G. Mahlabani, "The effects of building glass façade geometry on

wind infiltration and heating and cooling energy consumption," *Int. J. Technol.*, vol. 11, no. 2, pp. 235–247, 2020. https://doi.org/10.14716/ijtech.v11i2.3201

[33] C. Roselli, E. Marrasso, F. Tariello, and M. Sasso, "How different power grid efficiency scenarios affect the energy and environmental feasibility of a polygeneration system," *Energy*, vol. 201, p. 117576, 2020. https://doi.org/10.1016/J.ENERGY.2020.117576

[34] European Environment Agency, "Efficiency of conventional thermal electricity and heat production in Europe." https://www.eea.europa.eu/data-and-maps/indicators/efficiency-of-conventional-thermal-electricity-generation-4/assessment-2

[35] Nowtricity, "Current emissions in Norway." https://www.nowtricity.com/country/norway/#:~:text=Quick%20stats%20about%20Norway,countries%20in%20renewable%20energy%20production.

[36] S. Kokare, J. P. Oliveira, and R. Godina, "Life cycle assessment of additive manufacturing processes: A review," *J. Manuf. Syst.*, vol. 68, pp. 536–559, 2023. https://doi.org/10.1016/J.JMSY.2023.05.007

[37] ISO 14040:2006, "Environmental management—Life cycle assessment—Principles and framework," 2006. https://www.iso.org/obp/ui/#iso:std:iso:14040:ed-2:v1:en

[38] ISO 14040:2006, "Environmental management—Life cycle assessment—Requirements and guidelines," 2006. https://www.iso.org/standard/38498.html

[39] Kuraray Poval, "New LCA calculation CO2 footprint," 2025. https://www.kuraray-poval.com/it/

[40] American Chemistry Council, "Report: Shrinking environmental footprint in plastics manufacturing." https://www.americanchemistry.com/chemistry-in-america/news-trends/press-release/2022/report-shrinking-environmental-footprint-in-plastics-manufacturing

[41] S. Carlucci, F. Causone, F. De Rosa, and L. Pagliano, "A review of indices for assessing visual comfort with a view to their use in optimization processes to support building integrated design," *Renew. Sustain. Energy Rev.*, vol. 47, pp. 1016–1033, 2015. https://doi.org/10.1016/j.rser.2015.03.062

[42] openLCA Nexus. https://nexus.openlca.org/databases